ELSEVIER

Journal of Alloys and Compounds 450 (2008) 540–545

Journal of ALLOYS AND COMPOUNDS

www.elsevier.com/locate/jallcom

Novel alkaline-free Er^{3+}-doped fluorophosphate glasses for broadband optical fiber lasers and amplifiers

Ju H. Choi [a], Frank G. Shi [a,*], Alfred Margaryan [b], Ashot Margaryan [b], Wytze van der Veer [c]

[a] *Department of Chemical Engineering and Materials Science, University of California, Irivne, CA 92697, USA*
[b] *AFO Research Inc., Glendale, P.O. Box 1934, CA 91209, USA*
[c] *Department of Chemistry, University of California, Irivne, CA 92697, USA*

Received 20 March 2007; received in revised form 12 July 2007; accepted 14 July 2007
Available online 1 August 2007

Abstract

Two sets of Er^{3+}-doped alkaline-free glass systems, MgF_2–BaF_2–$Ba(PO_3)_2$–$Al(PO_3)_3$ (MBBA) and $Bi(PO_3)_3$–$Ba(PO_3)_2$–BaF_2–MgF_2 (BBBM), have been prepared and investigated with the aim of using them as active media. Radiative lifetimes (τ_{rad}) and branching ratios (β) have been obtained for the excited states of Er^{3+}. The absorption spectra were recorded to obtain the intensity parameters (Ω_t) which are found to be $\Omega_2 = 4.47 \times 10^{-20}$ cm^2, $\Omega_4 = 1.31 \times 10^{-20}$ cm^2, $\Omega_6 = 0.81 \times 10^{-20}$ cm^2 for the MBBA system and $\Omega_2 = 4.03 \times 10^{-20}$ cm^2, $\Omega_4 = 1.34 \times 10^{-20}$ cm^2, $\Omega_6 = 0.53 \times 10^{-20}$ for the BBBM system, respectively. The emission cross-section for the $^4I_{13/2} \rightarrow {}^4I_{15/2}$ transition is determined by the Fuchtbauer–Ladenburg method and found to be 2.35×10^{-20} cm^2 and 3.54×10^{-20} cm^2 for the MBBA and BBBM system, respectively. Comparison of the measured values to those of Er^{3+} transitions in other glass hosts suggests that our new glass systems are good candidates for broadband compact optical fiber and waveguide amplifier applications.

Keywords: Photonic glass; Erbium; Fiber laser; Fiber amplifier

1. Introduction

Er^{3+} is a well-known ion used in laser systems with transitions in the infrared region around 1550 nm ($^4I_{13/2} \rightarrow {}^4I_{15/2}$) for telecommunication applications, and 3000 nm ($^4I_{11/2} \rightarrow {}^4I_{13/2}$), for medical applications as well as in the green around 550 nm ($^4S_{3/2} \rightarrow {}^4I_{15/2}$) [1]. The $^4I_{13/2} \rightarrow {}^4I_{15/2}$ transition of Er^{3+} has been useful in optical devices such as the erbium-doped fiber amplifier (EDFA) which is applied in wavelength-division-multiplexing (WDM) transmission systems. In order to develop the most efficient optical amplifiers with broad, flat gain profiles, a number of active host matrices doped with the Er^{3+} ion have been investigated [2–5]. The host materials strongly influence the emission properties of Er^{3+} ions. Among the many possible host materials, fluorophospate glass has the advantages of low phonon energy, transmittance from UV to IR spectral range, and low nonlinear refractive index [6–10]. The fluorophosphate glass also has a better thermal stability and chemical durability than fluoride glasses due to the incorporation of phosphate [11]. In addition, the phosphate might provide multiple sites for rare earth dopants, allowing for a relatively high dopant concentration. In contrast to most host materials which are limited to low Er^{3+} ion concentration, fluorophosphate glasses enable the construction of short, highly efficient fiber or planar waveguide amplifiers [12]. In order to fabricate integrated optical amplifiers with small component dimensions, it is of significant importance to obtain the maximum gain and thus a large emission cross-section. In this work, two sets of Er^{3+}-doped alkaline-free MgF_2–BaF_2–$Ba(PO_3)_2$–$Al(PO_3)_3$ (MBBA system) and $Bi(PO_3)_3$–$Ba(PO_3)_2$–BaF_2–MgF_2 (BBBM system) are successfully developed with the aim of using them as active media with high gain. Based on these current glasses doped with Yb^{3+} and Nd^{3+}, the spectroscopic and optical properties have been already investigated according to their certain characteristics transition and show some potential application for laser media with high gain [13–18].

* Corresponding author. Tel.: +1 949 8245362; fax: +1 949 8242541.
E-mail address: fgshi@uci.edu (F.G. Shi).

0925-8388/$ – see front matter © 2007 Elsevier B.V. All rights reserved.
doi:10.1016/j.jallcom.2007.07.094

In order to access the potential for laser media, we conducted a systematic investigation of the spectroscopic properties of Er^{3+}-doped MBBA system for the first project and then the modified new system of the BBBM systems has been developed. The main objective is to develop new host materials with a large bandwidth and a high emission cross-section. Initially we obtained intensity parameters which are used to calculate the spontaneous emission probabilities and branching ratios from the excited-state J manifolds to the lower-lying J' manifolds. Next, the radiative lifetime for the $^4I_{13/2}$ metastable level is determined to obtain the spectral dependence of the stimulated emission cross-section and gain coefficient for the $^4I_{13/2} \rightarrow {}^4I_{15/2}$ transition, which is of special interest for laser applications. Finally, the potential of these systems as laser media is evaluated by comparison to other reported glass host.

2. Experiments and data analysis

The glasses $40MgF_2$–$40BaF_2$–$10Ba(PO_3)_2$–$10Al(PO_3)_3$ and $20Bi(PO_3)_3$–$10Ba(PO_3)_2$–$35BaF_2$–$35MgF_2$ were prepared from reagent-grade materials (City Chemicals, except for Er_2O_3, Spectrum Materials), all have better than 99.99% purity. The ingredients of the glasses were weighed with 0.1% accuracy and mixed thoroughly for 3 h. Next, the raw mixed materials were melted in a vitreous carbon crucible in Ar-atmosphere at 1200 °C. The melt was quenched by pouring it in a room temperature stainless steel mold. Next, the samples were annealed below the glass transition temperature, around 400 °C, to remove internal stress, which was verified by examination with a polariscope (Rudolph Instruments). The samples for optical and spectroscopic measurements were cut and polished to a size of 15 mm × 10 mm × 2 mm.

The refractive index n_d of the samples was measured at 588 nm, using an Abbe refractometer (ATAGO). The absorption spectra were obtained at room temperature in the range of 400–1700 nm with a Perkin-Elmer photo spectrometer (Lambda 900). The lifetime and fluorescence spectrum of both samples was recorded using a chopped Ti-Sapphire laser (Coherent 890) tuned to 800 nm, pumped by the 514 nm line of an Ar laser (Innova 300). The fluorescence signal was recorded with a 0.25 m monochromator (Oriel 77200), using a InGaAs PIN detector (Thorlabs DET 410), a trans-impedance amplifier and a Lock-In amplifier (Oriel Merlin 70100). The lifetimes of both samples, was recorded with the same system, recording the temporal behavior of the fluorescence signal with a 100 MHz digital Oscilloscope.

3. Results and discussion

3.1. Absorption spectra and oscillator strength

Fig. 1 shows the absorption cross-section of the Er^{3+}-doped MBBA and BBBM systems in the spectral region of 400–1700 nm. The obtained absorption spectra for the MBBA and BBBM systems are very similar. They both show groups of lines, which correspond to transitions between the ground state $^4I_{15/2}$ and excited states in the $4f^{11}$ electronic configuration of the Er^{3+} ion. The radiative nature of trivalent rare earth ions in a variety of laser host materials is usually investigated using the Judd-Ofelt model [19,20]. In this model the absorption spectra and the radiative properties of the rare earth ions are explained using the electric dipole (ed), magnetic dipole (md) and electric quadrupole (eq) transition probabilities of the 4f–4f electronic transitions. The observed oscillator strengths f_{med} at each absorption peak is calculated by integration the optical absorption spectra over each peak, as given by following expression:

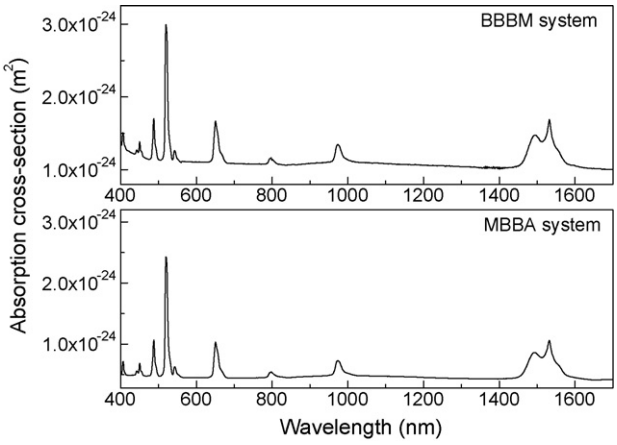

Fig. 1. Optical absorption cross-section in the BBBM and MBBA systems.

$$f_{med} = \frac{mc^2}{\pi e^2 N} \int \frac{\alpha(\lambda)}{\lambda^2} d\lambda \quad (1)$$

Here c is the velocity of light and N is the Er^{3+} ion concentration (ion/cm^3). $\alpha(\lambda)$ (= $2.303D_o(\lambda)/d$) is the optical absorption coefficient at a particular absorption wavelength λ, which is calculated from the sample thickness d and the measured absorption density $D_o(\lambda)$. The oscillator strengths as predicted by Judd-Ofelt model f_{cal} were also calculated. The oscillator strengths of the observed electronic transition are due to three interactions, electrical dipole (ed), magnetic dipole (md) and electric quadrupole (eq). In most instances in the Er^{3+} system, the oscillator strength of the eq component is of the order of 10^{-10}, and the md component is of the order of 10^{-8}. These contributions are thus unimportant compared with the ed contribution to the oscillator strength, which is in the order of 10^{-6} [1]. However, a significant contribution of the md component is involved for the $^4I_{15/2} \rightarrow {}^4I_{13/2}$ absorption transition for the Er^{3+}. Therefore, theoretical oscillator strengths $f(aJ, bJ')$ of the $J \rightarrow J'$ transition at the mean frequency ν is given for both the electric and the magnetic dipole transition by the following equation

$$f_{cal}(aJ, bJ') = \frac{8\pi^2 m\nu}{3(2J+1)he^2n^2}[\chi_{ed}S_{ed}(aJ, bJ') + \chi_{md}S_{md}(aJ, bJ')] \quad (2)$$

where m is the mass of the electron and e and h are the charge of the electron and plank's constant, respectively. $\chi_{ed} = n(n^2+2)^2/9$ and $\chi_{md} = n^3$ are local field corrections and are functions of the refractive index n of the medium. S_{ed} and S_{md} are the electrical

Table 1
Values of reduced matrix elements for the absorption transitions of Er^{3+}

Transitions	$[U^{(2)}]^2$	$[U^{(4)}]^2$	$[U^{(6)}]^2$
$^4I_{13/2} \rightarrow {}^4I_{15/2}$	0.0195	0.1173	1.4316
$^4I_{11/2} \rightarrow {}^4I_{13/2}$	0.0331	0.1708	1.0864
$^4I_{11/2} \rightarrow {}^4I_{15/2}$	0.0282	0.0003	0.3953
$^4I_{9/2} \rightarrow {}^4I_{11/2}$	0.003	0.0674	0.1271
$^4I_{9/2} \rightarrow {}^4I_{13/2}$	0.0004	0.0106	0.7162
$^4I_{9/2} \rightarrow {}^4I_{15/2}$	0	0.1732	0.0099
$^4F_{9/2} \rightarrow {}^4I_{9/2}$	0.1279	0.0059	0.0281
$^4F_{9/2} \rightarrow {}^4I_{11/2}$	0.0704	0.0112	1.2839
$^4F_{9/2} \rightarrow {}^4I_{13/2}$	0.0101	1.5333	0.0714
$^4F_{9/2} \rightarrow {}^4I_{15/2}$	0	0.5354	0.4619
$^4S_{3/2} \rightarrow {}^4I_{9/2}$	0	0.0788	0.2542
$^4S_{3/2} \rightarrow {}^4I_{11/2}$	0	0.0042	0.0739
$^4S_{3/2} \rightarrow {}^4I_{13/2}$	0	0	0.3462
$^4S_{3/2} \rightarrow {}^4I_{15/2}$	0	0	0.2211
$^2H_{11/2} \rightarrow {}^4F_{9/2}$	0.3629	0.0224	0.0022
$^2H_{11/2} \rightarrow {}^4I_{9/2}$	0.2077	0.0662	0.2858
$^2H_{11/2} \rightarrow {}^4I_{11/2}$	0.0357	0.1382	0.0371
$^2H_{11/2} \rightarrow {}^4I_{13/2}$	0.023	0.0611	0.0527
$^2H_{11/2} \rightarrow {}^4I_{15/2}$	0.7125	0.4123	0.0925

Table 2
Measured line strength and calculated line strength of Er^{3+} in MBBA and BBBM systems

Energy level	MBBA		BBBM	
From $^4I_{15/2}$	Calculated	Measured	Calculated	Measured
$^4I_{13/2}$	0.22	0.35	0.20	0.28
$^4I_{11/2}$	0.44	0.60	0.33	0.61
$^4I_{9/2}$	0.54	0.27	0.41	0.22
$^4F_{9/2}$	0.35	1.99	0.37	1.92
$^4S_{3/2}$	1.93	0.33	1.83	0.31
$^2H_{11/2}$	0.33	7.09	0.23	6.87
$^4F_{7/2}$	7.61	1.90	7.42	1.77
$^2G_{9/2}$	1.52	0.34	1.24	0.07
$^2F_{3/2}$	0.40	0.19	0.28	0.12
$^2G_{9/2}$	0.25	0.71	0.18	0.43
RMS ($\times 10^{-6}$)	8.52		6.57	

dipole and the magnetic dipole line strength, respectively and are given by the following equations

$$S_{ed}(aJ, bJ') = e^2 \sum_{t=2,4,6} \Omega_t \left| \left\langle 4f^N aJ || U^{(t)} || 4f^N bJ' \right\rangle \right|^2 \quad (3)$$

$$S_{md}(aJ, bJ') = \frac{e^2\hbar^2}{4m^2c^2} \left| \left\langle 4f^N aJ || \overrightarrow{L} + 2\overrightarrow{S} || 4f^N bJ' \right\rangle \right|^2 \quad (4)$$

The reduced matrix elements of the unit tensor operator, $\langle || U^{(t)} || \rangle$, are calculated in the intermediate-coupling approximation. They are found to be almost invariant to the environment and are given in Table 1 [21]. The observed and calculated line strengths of Er^{3+} transitions from ground state $^4I_{15/2}$ to upper states in the ^4S, ^4F, ^4I as well as the ^2G and ^2H electronic configurations are summarized in Table 2 for both the MBBA, and BBBM system.

As can be seen from this table, at a number of instances the calculated (electric dipole only) values and the measured values show a discrepancy. This can be explained as the effect of magnetic dipole interaction. The $^4I_{15/2} \rightarrow {}^4I_{13/2}$ transition is of special interest because of applications of the MBBA and BBBM materials in laser systems. The measured line strengths of this transition are 0.35×10^{-6} and 0.28×10^{-6} while the calculated (electric dipole only) values are 0.22×10^{-6} and 0.20×10^{-6}, respectively. The difference between these values, the magnetic dipole component of the line strength is thus in this case 0.13×10^{-6} and 0.08×10^{-6}, respectively.

3.2. Intensity parameter and quality factor

The Judd-Ofelt intensity parameters were determined by a least squares fit of the theoretical (free ion) oscillator strengths to the measured (glass matrix) values obtained from optical absorption spectra. In order to evaluate the quality of this fit, the root-mean-square (rms), of the deviation was obtained (δ_{rms}):

$$\delta_{rms} = \left[\frac{\sum (f_{cal} - f_{med})^2}{\sum f_{med}^2} \right]^{1/2} \quad (5)$$

By fitting the measured oscillator strengths f_{med} to the calculated values f_{cal} we obtained the following values for three Judd-Ofelt parameters Ω_2, Ω_4 and Ω_6: $\Omega_2 = 4.47 \times 10^{-20}\,cm^2$, $\Omega_4 = 1.31 \times 10^{-20}\,cm^2$ and $\Omega_6 = 0.81 \times 10^{-20}\,cm^2$ for the MBBA system and $\Omega_2 = 4.03 \times 10^{-20}\,cm^2$, $\Omega_4 = 1.34 \times 10^{-20}\,cm^2$ and $\Omega_6 = 0.53 \times 10^{-20}$ for the BBBM system. The deviation δ_{rms} of the fits was 8.52×10^{-6} and 6.57×10^{-6}, respectively, which indicates that these fits are reliable. In Table 3 [2,22–24] these values are compared to those for other reported laser glasses. The value of Ω_2 indicates the strength of the covalent binding between the tri-valent rare earth ion and the host material [25,26]. The values of Ω_2 of the MBBA and BBBM systems are smaller than those of BK20 oxide glass and phosphate glass, which show strong co-valent bonds. The measured value

Table 3
Comparison of Judd-Ofelt parameters of Er^{3+}-doped MBBA and BBBM system with other reported laser glasses

Glasses	Ω_2 ($\times 10^{-20}\,cm^2$)	Ω_4 ($\times 10^{-20}\,cm^2$)	Ω_6 ($\times 10^{-20}\,cm^2$)	4/6	Refs.
BK20	5.66	1.84	1.18	1.56	[23]
ZBLAN	2.20	1.40	0.91	1.54	[24]
Phosphate	6.65	1.52	1.11	1.34	[25]
FP20	4.71	1.61	1.62	0.99	[1]
MBBA	4.47	1.31	0.81	1.62	Current work
BBBM	4.03	1.34	0.53	2.53	

Table 4
Comparison of the predicted radiative lifetime of Er^{3+} in MBBA and BBBM systems with other reported laser glasses

Excited state	Phosphate	ZBLA	Silicate	FP20	MBBA	BBBM
$^4I_{13/2}$	9.96	9.20	7.30	6.80	11.03	10.39
$^4I_{11/2}$	6.14	9.20	5.81	5.68	10.55	11.20
$^4I_{9/2}$	7.78	8.30	4.85	5.95	6.73	6.13
$^4F_{9/2}$	0.88	0.92	0.72	0.69	0.88	0.79
$^4S_{3/2}$	0.56	0.86	0.78	0.53	1.36	1.20
$^2H_{11/2}$	0.12	0.31	0.10	0.17	0.17	0.15
Refs.	[28]	[29]	[30]	[2]	Current works	

is higher than that of ZBLAN, which has a very high fluoride content causing strong ionic bonds and thus weaker co-valent bonds. The values of Ω_2 of the MBBA, and BBBM system are comparable to those of other fluorophosphate glass with similar fluorine content.

The effect of co-valent bonding between the Er^{3+} ions and the host material can be understood in terms of the Judd-Ofelt parameters. In case of a Er^{3+}-doped system the $t=2$ transition matrix elements $[U^{(2)}]^2$ of the transitions between the $^4I_{11/2}$, $^4I_{13/2}$ and $^4I_{15/2}$ states are very small (see Table 1). The quality of these transitions for laser operation is thus characterized by Ω_4 and Ω_6 via the spectroscopic quality factor Q ($=\Omega_4/\Omega_6$), as introduced by Kaminskii [27]. The Q values are found to be 1.62 and 2.53 for the MBBA and BBBM system, respectively. These values are larger than those found in most laser glasses as well as in FP20, see Table 3. The MBBA and BBBM glasses are thus better suitable for laser applications than other published glass systems.

3.3. Spontaneous emission probabilities branching ratios and radiative lifetimes

An important factor in determining the suitability of a trivalent ion-doped glass for laser operation is the spontaneous emission probability (A_{ra}) of the laser transition. The relation between this probability and the electric dipole and magnetic dipole line strengths (S_{ed} and S_{md}) is given by the following equation

$$A(aJ : bJ') = \frac{64\pi^4 v^3}{3h(2J+1)c^3}(\chi_{ed}S_{ed} + \chi_{md}S_{md}) \quad (6)$$

where J', J are the total momentum for the upper and lower levels. The predicted radiative lifetimes (τ_{rad}) of excited states of Er^{3+} are related to the emission probability of each transition from the initial J state to the final J' manifold. They are determined from the following relation:

$$\tau = \frac{1}{\sum_{J'} A(J \rightarrow J')} \quad (7)$$

where the sum runs over all final states J'. The values of the predicted radiative lifetimes are listed for a number of host materials in Table 4 [2,28–30]. The values of τ_{rad} of the $^4I_{13/2}$ state are found to be 11.03 ms and 10.39 ms for the MBBA and BBBM system, respectively. They are within the range of other laser host glasses doped with Er^{3+}which have literature values in the 2.3–11 ms range [31,32]. The luminescence branching ratios are a very important parameter for verifying the applicability of a material for laser operation. In principle the branching ratio of the transition between the upper states to the lower laser state should be as high as possible; the competition for the popula-

Table 5
Calculated spontaneous emission probabilities, and fluorescence branching ratios in the MBBA and BBBM system

Transitions	Energy (cm^{-1})	MBBA		BBBM	
		$A_{JJ'}$ (s^{-1})	β	$A_{JJ'}$ (s^{-1})	β
$^4I_{13/2} \rightarrow {}^4I_{15/2}$	6517	50.87 (ed), +39.81 (md)	1.000	54.58 (ed), +41.67 (md)	1.000
$^4I_{11/2} \rightarrow {}^4I_{13/2}$	3750	10.62 (ed), +8.89 (md)	0.113	11.31 (ed), +9.31 (md)	0.121
$^4I_{11/2} \rightarrow {}^4I_{15/2}$	10277	75.26	0.803	82.02	0.875
$^4I_{9/2} \rightarrow {}^4I_{15/2}$	2206	0.47 (ed), +1.27 (md)	0.003	0.50 (ed), +1.33 (md)	0.003
$^4I_{9/2} \rightarrow {}^4I_{13/2}$	5956	21.40	0.135	22.92	0.144
$^4I_{9/2} \rightarrow {}^4I_{11/2}$	12484	124.11	0.782	136.96	0.863
$^4F_{9/2} \rightarrow {}^4I_{9/2}$	2876	3.26 (ed), +6.25 (md)	0.003	3.47 (ed), +6.54 (md)	0.003
$^4F_{9/2} \rightarrow {}^4I_{11/2}$	5083	32.85 (ed), +2.75 (md)	0.027	35.10 (ed), +2.88 (md)	0.029
$^4F_{9/2} \rightarrow {}^4I_{13/2}$	6527	157.66	0.129	169.15	0.139
$^4F_{9/2} \rightarrow {}^4I_{15/2}$	15360	935.75	0.767	1053.25	0.863
$^4S_{3/2} \rightarrow {}^4I_{9/2}$	5965	33.19	0.042	35.55	0.045
$^4S_{3/2} \rightarrow {}^4I_{11/2}$	8172	15.76	0.020	17.01	0.022
$^4S_{3/2} \rightarrow {}^4I_{13/2}$	11922	200.78	0.255	220.81	0.280
$^4S_{3/2} \rightarrow {}^4I_{15/2}$	18450	484.06	0.614	559.02	0.709
$^2H_{11/2} \rightarrow {}^4F_{9/2}$	3838	17.92 (ed), +0.25 (md)	0.003	19.09 (ed), +0.2 (md)	0.003
$^2H_{11/2} \rightarrow {}^4I_{9/2}$	6709	69.44	0.011	74.55	0.012
$^2H_{11/2} \rightarrow {}^4I_{11/2}$	10277	82.82 (ed), +100.36 (md)	0.014	90.26 (ed), +105.07 (md)	0.015
$^2H_{11/2} \rightarrow {}^4I_{13/2}$	12666	90.02 (ed), +67.12 (md)	0.015	99.46 (ed), +70.27 (md)	0.016
$^2H_{11/2} \rightarrow {}^4I_{15/2}$	19193	5417.08	0.896	6298.90	1.042

tion in the upper laser state should be as small as possible. The branching ratio of the transitions from the upper state aJ to lower levels bJ' is given by the following equation

$$\beta(aJ : bJ') = \frac{A(aJ : bJ')}{\sum_{J'} A(aJ : bJ')} \tag{8}$$

The spontaneous transition probabilities and the branching ratios of transitions from the $^4I_{13/2}$, $^4I_{11/2}$, $^4I_{9/2}$, $^4F_{9/2}$, $^4S_{3/2}$ and $^2H_{11/2}$ upper states to all relevant lower states were calculated using Eqs. (6) and (7), they are listed in Table 5. Since the $^4I_{15/2}$ state is the only electronic state below the $^4I_{13/2}$ state, the branching ratio of this transition is unity, making this transition highly suitable for low loss laser generation at 1536 nm. The most convenient route for pumping this level is via the $^4I_{11/2}$ state, forming a three level laser system. The branching ratio of the $^4I_{11/2} \rightarrow {}^4I_{15/2}$ transition was found to be 0.803 in MBBA system and 0.875 in BBBM system, effectively enabling a highly efficient laser scheme (see Table 5).

Other transitions with a large branching ratio are $^4S_{3/2} \rightarrow {}^4I_{15/2}$ (61.4% in MBBA and 70.9% in BBBM) and $^4F_{9/2} \rightarrow {}^4I_{15/2}$ (76.7% in MBBA system and 86.3% in BBBM system). Thus, it is expected that these transition can be used to efficiently obtain green (542 nm) and red (651 nm) emission under suitable excitation conditions, which includes an up-conversion excitation scheme. A detailed study on up-conversion emission generation using this system will be discussed in a forthcoming paper.

3.4. The emission cross-section and gain coefficient of the $^4I_{13/2} \rightarrow {}^4I_{15/2}$ transition

The efficiency of a laser transition is evaluated by considering stimulated emission cross-section ($\sigma_{em}(\lambda)$). In our case $\sigma_{em}(\lambda)$ was determined from the emission spectrum using Fuchtbauer–Ladenburg method [33]

$$\sigma_{em} = \frac{\beta_{J \rightarrow J'} \lambda_p^4 A_{ra}}{8\pi c n (\lambda_p)^2 \Delta\lambda_{eff}} \tag{9}$$

where λ_p is the peak wavelength of the emission, λ_{eff} is the width of the emission line, $\beta_{J \rightarrow J'}$ is the branching ratio, which

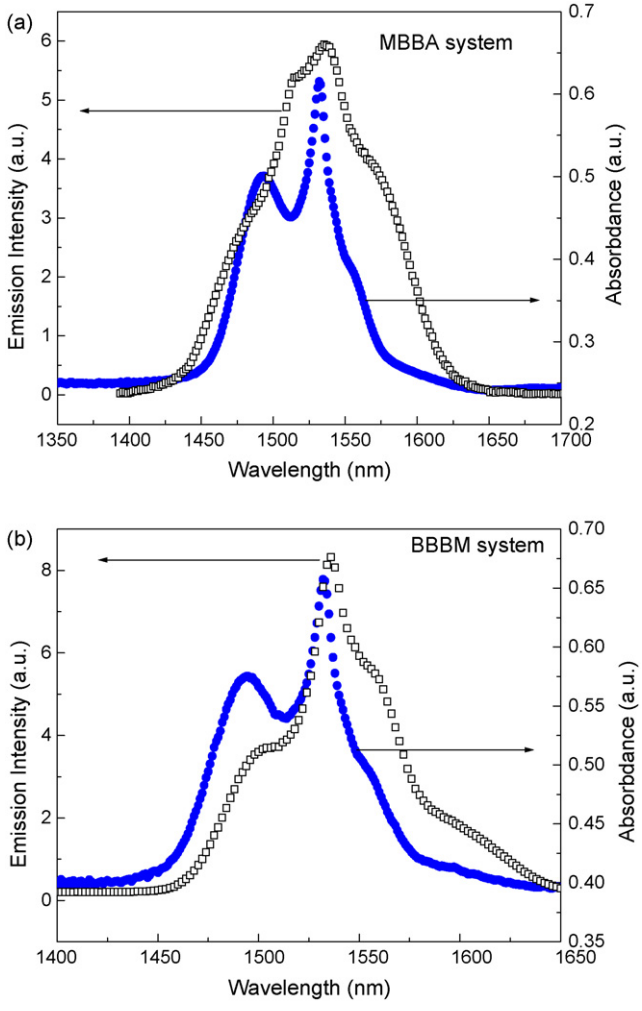

Fig. 2. Absorption cross-section and measured emission cross-section of Er^{3+} in (a) the MBBA system and (b) the BBBM system.

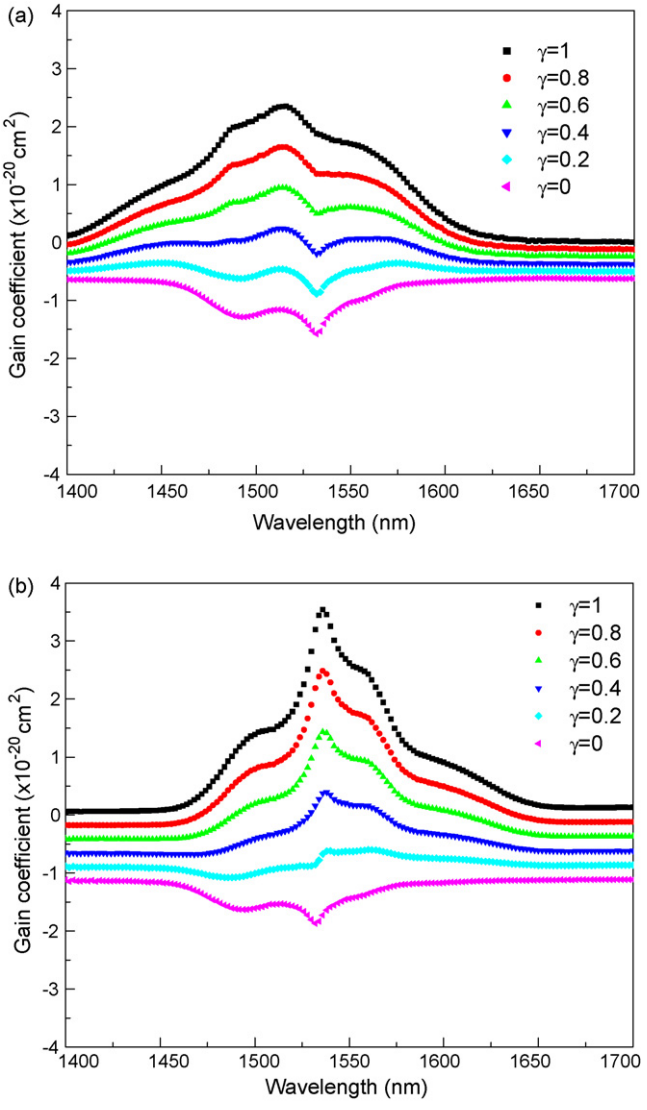

Fig. 3. Gain coefficient in the eye-safe range of Er^{3+} in (a) the MBBA system and (b) the BBBM system.

is in case of the $^4I_{13/2} \rightarrow {}^4I_{15/2}$ transition equal to 1, c is the speed of light in vacuums, and $n(\lambda_p)$ is the refractive index at emission peak wavelength. In our case an effective line width is used instead of the full width at half maximum to compensate for the a-symmetric profile of the emission line. Fig. 2 shows the absorption cross-section, $\sigma_{abs}(\lambda)$, and the emission cross-section, $\sigma_{em}(\lambda)$, determined by Fuchtbauer–Ladenburg method. For the MBBA and BBBM system, the peak absorption cross sections $\sigma_{abs}(\lambda)$ turned out to be 1.58×10^{-20} cm^2 and 1.87×10^{-20} cm^2 and the peak emission cross sections $\sigma_{em}(\lambda)$ are 1.86×10^{-20} cm^2 and 3.14×10^{-20} cm^2, respectively.

Comparing the Er^{3+} ion to a simplified two level system, we assume the population is either in the $^4I_{15/2}$ ground state or the $^4I_{13/2}$ excited state. In this case the optical gain properties are directly associated with the absorption and emission cross sections. Gain spectra is shown in Fig. 3 as a function of the population inversion γ, using the relation below

$$G(\lambda) = \gamma\sigma_{em}(\lambda) - (1 - \gamma)\sigma_{abs}(\lambda) \quad (10)$$

Using this equation, and the observed cross sections for the MBBA and BBBM system, we calculated the gain spectra as shown in Fig. 3. Note that the gain will be positive at 1536 nm and 1516 nm, when the population inversion is larger than 0.5 and 0.6, respectively. The maximum value for the gain is achieved in the case of complete population inversion ($\gamma = 1$), in this case cross-section for stimulated emission is 2.35×10^{-20} cm^2 and 3.54×10^{-20} cm^2 for the MBBA and BBBM system, respectively.

4. Conclusion remarks

The novel MBBA and BBBM systems were successfully developed and the absorption and emission spectra of Er^{3+} were measured and analyzed. The intensity parameters, the radiative lifetime, branching ratio and the fluorescence lifetime were calculated from and the absorption and emission spectra and compared with other laser glasses. Three intensity parameters are found to be $\Omega_2 = 4.47 \times 10^{-20}$ cm^2, $\Omega_4 = 1.31 \times 10^{-20}$ cm^2, $\Omega_6 = 0.81 \times 10^{-20}$ cm^2 for MBBA system and $\Omega_2 = 4.03 \times 10^{-20}$ cm^2, $\Omega_4 = 1.34 \times 10^{-20}$ cm^2, $\Omega_6 = 0.53 \times 10^{-20}$ for BBBM system, respectively. For the MBBA and BBBM system, strong emission bands were observed at 1536 nm and 1516 nm and the effective bandwidths were found to be 91 nm and 64 nm, respectively. Emission cross-section determined by Fuchtbauer–Ladenburg method for the $^4I_{13/2} \rightarrow {}^4I_{15/2}$ transition are found to be 2.35×10^{-20} cm^2 and 3.54×10^{-20} cm^2 and population inversion of above 50% and 60% were obtained for the MBBA and BBBM system, respectively. These spectroscopic results show that these novel materials are strong candidates for developing broadband optical amplifiers and compact fiber lasers.

References

[1] A. Lira, C.I. Camarillo, E. Camarillo, F. Ramos, M. Flores, U. Caldino, J. Phys. Condens. Matter 18 (2004) 5925.
[2] H. Ebendorff-Heidepriem, D. Ehrt, M. Bettinelli, A. Speghini, J. Non-Cryst. Solid 240 (1998) 66.
[3] S. Jiang, M. Myers, N. Peyghambarian, J. Non-Cryst. Solid 143 (1998) 239.
[4] Y. Ding, S. Jiang, B.C. Hwang, T. Luo, N. Peyghambarian, Y. Himei, T. Ito, Y. Miura, Opt. Mater. 15 (2000) 123.
[5] S.Q. Man, S.F. Wong, E.Y.B. Pun, J. Opt. Soc. Am. B. 19 (2002) 1839.
[6] S.V.J. Lakshman, Y.C. Ratnakaram, Phys. Chem. Glasses 29 (1988) 26.
[7] B. Viana, M. Palazzi, O. LeFol, J. Non-Cryst. Solids 215 (1997) 96.
[8] S. Jiang, T. Luo, B.C. Hwang, F. Smekatala, K. Seneschal, J. Lucas, N. Peyghambarian, J. Non-Cryst. Solids 263 (2000) 364.
[9] B. Kumar, R. Harris, Phys. Chem. Glasses 25 (1984) 155.
[10] S.E. Stokowski, W.E. Martin, S.M. Yarema, J. Non-Cryst. Solids 40 (1980) 481.
[11] M. Matecki, M. Poulain, J. Non-Cryst. Solids 56 (1983) 111.
[12] A. Mori, Y. Ohishi, S. Sudo, Electron. Lett. 33 (1997) 863.
[13] J. Choi, A. Margaryan, A. Margaryan, W. van der Veer, F.G. Shi, Adv. OptoElectron. 8 (2007), article ID 39892.
[14] A. Margaryan, J.H. Choi, A. Margaryan, F. Shi, Appl. Phys. B. Laser Opt. 78 (2004) 409.
[15] J.H. Choi, F.G. Shi, A. Margaryan, A. Margaryan, Mater. Res. Bull. 40 (2005) 2189.
[16] J.H. Choi, F.G. Shi, A. Margaryan, A. Margaryan, J. Lumin. 114 (2005) 167.
[17] J.H. Choi, F.G. Shi, A. Margaryan, A. Margaryan, J. Alloys Compd. 396 (2005) 79.
[18] J.H. Choi, F.G. Shi, A. Margaryan, A. Margaryan, J. Mater. Res. 20 (2005) 264.
[19] B.R. Judd, Phys. Rev. 127 (1962) 750.
[20] G.S. Ofelt, J. Chem. Phys. 37 (1962) 511.
[21] W.T. Carnall, J.P. Hessler, F.W. Wagner, J. Phys. Chem. 82 (1978) 2152.
[22] S. Tanabe, T. Ohyagi, N. Soga, T. Hanada, Phys. Rev. B 46 (1992) 3305.
[23] J. McDougall, D.B. Hollios, M.J. Payne, Phys. Chem. Glasses 37 (1996) 73.
[24] X. Zou, T. Izumitani, J. Non-Cryst. Solid 162 (1993) 68.
[25] R.R. Jacobs, M.J. Weber, IEEE J. Quantum Electron. 12 (1976) 102.
[26] A.K. Jorgensen, R. Reisfeld, J. Less-Common Met. 93 (1983) 107.
[27] A.A. Kaminskii, Laser Crystals, Their Physics and Properties, Springer, Berlin, 1975.
[28] D.K. Sardar, J.B. Gruber, B. Zandi, J.A. Hutchinson, C.W. Trussell, J. Appl. Phys. 93 (2003) 2041.
[29] M.D. Shinm, W.A. Sibley, M.G. Drexhage, R.N. Brown, Phys. Rev. B 27 (1983) 6635.
[30] M.P. Hehlen, N.J. Cockroft, T.R. Gosnell, A.J. Bruce, Phys. Rev. B 56 (1997) 9302.
[31] M.J. Weber, Phys. Rev. 157 (1967) 262.
[32] J. Amin, B. Dussardier, T. Schweizer, M. Hempstead, J. Lumin. 69 (1996) 17.
[33] C.B. Layne, W.H. Lowdermilk, M.J. Weber, Phys. Rev. B 16 (1977) 10.